Title

Droplet Ejection at Controlled Angles via Acoustofluidic Jetting

Journal

Physical Review Letters, 125(18)

ISSN

0031-9007

Authors

Connacher, William
Orosco, Jeremy
Friend, James

Publication Date

2020-10-30

DOI

10.1103/physrevlett.125.184504

Peer reviewed

Droplet Ejection at Controlled Angles via Acoustofluidic Jetting

William Connacher, Jeremy Orosco, and James Friend*
Medically Advanced Devices Laboratory, in the Center for Medical Devices Department of Mechanical and Aerospace Engineering, Jacobs School of Engineering, Department of Surgery, School of Medicine University of California San Diego, La Jolla, California 92093, USA

(Received 16 April 2020; revised 22 July 2020; accepted 11 September 2020; published 30 October 2020)

We study the nozzle-free ejection of liquid droplets at controlled angles from a sessile drop actuated from two, mutually opposed directions by focused surface acoustic waves with dissimilar parameters. Previous researchers assumed that jets formed in this way are limited by the Rayleigh angle. However, when we carefully account for surface tension in addition to the driving force, acoustic streaming, we find a quantitative model that reduces to the Rayleigh angle only when inertia is dominant, and suggests larger ejection angles are possible in many practical situations. We confirm this in demonstrating ejection at more than double the Rayleigh angle. Our model explains the effects of both fluid and input parameters on experiments with a range of liquids. We extract, from this model, a dimensionless number that serves as an analog for the typical Weber number for predicting single droplet events.

DOI: 10.1103/PhysRevLett.125.184504

Introduction.—Acoustofluidic jetting, droplet ejection without an orifice from a sessile parent drop by surface acoustic wave (SAW) actuation [1], requires deeper physical understanding to gain quantitative control. There are exciting applications [2–4], including swifter printing by replacing nozzle translation with ejection angle control. Ejection angle control physics are unexplored, with only modest control previously achieved via variation of acoustic power from opposite sides of a sessile drop [5]. The driving force of the phenomenon, acoustic streaming, has been well studied [6]. Tan *et al.* studied vertical jetting using now typical devices [1] [Fig. 1(a)] producing two counter-propagating SAW. Interdigital transducers (IDTs) produce SAW that "leaks" energy into liquid as longitudinal sound waves. These propagate at the Rayleigh angle, θ_R, measured from vertical [Fig. 1(b)], to produce momentum flux driven streaming from viscous attenuation [7]. The value of $\theta_R = \sin^{-1}(c_l/c_r)$ is determined by the mismatch in velocity between that of the surface acoustic wave, c_r, and that of the sound wave in the liquid, c_l.

The current assumption for ejection angle control is flawed because it fails to account for surface tension. Streaming forms a Gaussian jet at θ_R in a fluid half-space [8]. In sessile drops, however, interfacial forces must be considered. Castro *et al.* assumed that jetting from a single IDT SAW source occurs strictly at θ_R [5] as reported by Shiokawa *et al.* [9]. This limits the range of the ejection angle, defined by θ_e from the vertical, to between $-\theta_R$ and $+\theta_R$ from the vertical when using two parallel IDT SAW sources. For water and SAW on lithium niobate (LN), $\theta_R = 22°$. With demonstrated control so far limited to $\theta_e = \pm 15°$, this assumption seems reasonable, especially without quantitative modeling [5].

However, experimentation reveals that the ejection angle, θ_e, can be much larger than θ_R. Droplets eject from one SAW source at the "limiting angle" $\theta_e = \theta_R = 22°$ only when the vibration velocity is large. The ejection angle, θ_e, becomes larger than the Rayleigh angle, θ_R, when the vibration velocity is reduced (see Fig. 2)

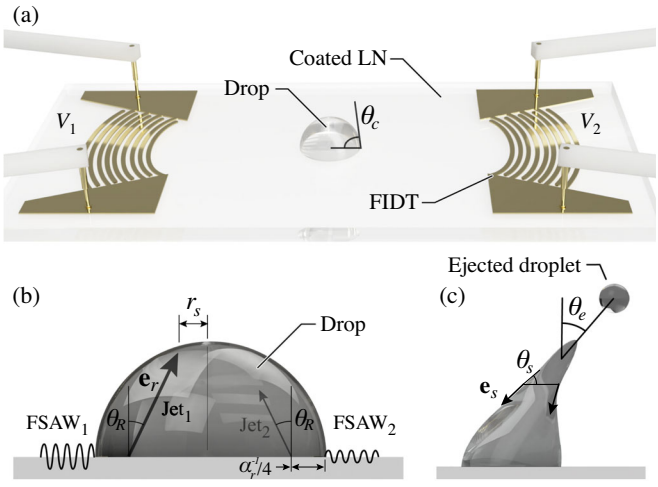

FIG. 1. (a) Typical acoustofluidic jetting devices consist of two focused IDTs (FIDTs), which produce focusing SAW (FSAW). A sessile drop with a given volume is confined to the SAW focal region by a hydrophobic coating that is applied everywhere except this region. The resulting contact angle, θ_c, depends on the size of the region. A voltage, V_i, signal with burst duration t is delivered to each FIDT. (b) A stationary sessile drop is deformed by acoustic streaming when SAW leaks in at the Rayleigh angle, θ_R, while (c) surface tension resists deformation according to Eq. (3) resulting in an ejected droplet at θ_e.

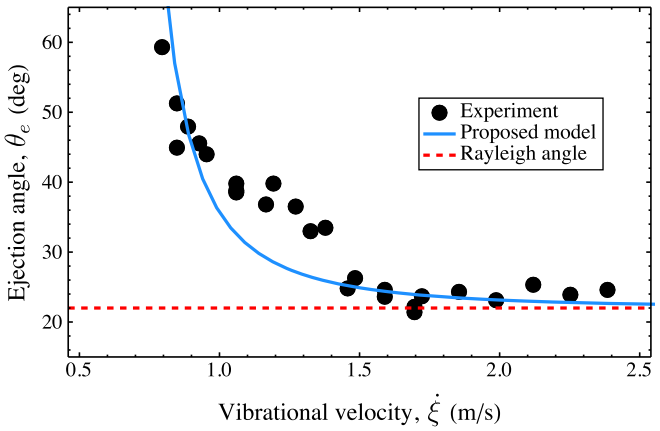

FIG. 2. As vibrational velocity, $\dot{\xi}$, due to one FIDT is increased, θ_e approaches θ_R from larger angles. This result is at odds with the assumption in the literature that θ_R is the upper limit. Instead, it appears to be the lower limit in the case of a single IDT SAW source. Our proposed model (see text) provides a fuller understanding of these physical trends when two SAW sources are considered.

when the vibration velocity is reduced. This contradicts the assumption that θ_R limits θ_e and demands a more complete description. Figure 2 demonstrates that a balance between inertia and surface tension yields asymptotic dynamics: when inertia dominates, droplets eject near θ_R, but when surface tension dominates, droplets eject at significantly greater angles.

Why does surface tension change the ejection angle, θ_e, rather than directly oppose inertia? Recalling the classic text by de Gennes *et al.* (see Supplemental Material for a helpful analog) [10], surface tension produces a force per unit length tangent to the fluid interface and opposing surface area generation. In our system [Fig. 1(b)], generally the fluid interface does not align with inertia, thus, surface tension modifies θ_e. This explains why Shiokawa *et al.* observed jetting at the Rayleigh angle: (i) the hydrophobic surface made it a special case where the fluid interface was nearly perpendicular to inertia, and (ii) a large inertia was used, which dominated surface tension.

We are also interested in which parameters produce a single droplet rather than zero or multiple. Tan *et al.* acknowledge surface tension's role in opposing inertia and define a Weber number, $\mathrm{We}_j \equiv [(\rho_l U_j^2 R_j)/\gamma]$, distinguishing zero, one, or multiple droplet jetting events [1]. However, $\mathrm{We}_j = 1$ does not align with experimental single-droplet ejection conditions. The definition also requires advance knowledge of the jet velocity, U_j, and jet radius, R_j, precluding ejection prediction. Castro *et al.* defined [11] $\mathrm{We}' \equiv [(VI\Delta t)/(\pi\gamma L^2)]$, without explicit consideration of the acoustofluidic physics (note that they issued a correction to their original equation in [11]). Rayleigh, Plateau, and others have thoroughly studied droplet formation—Eggers provides two elucidating reviews [12,13]—but the majority of this research involves an orifice or nozzle. Therefore, it is unsurprising that We_j relies on U_j and R_j; typical Weber numbers use orifice-dependent length scales and fluid velocities entering the nozzle, each typically defined by the researcher in droplet breakup studies. In our case, the corresponding choices are not obvious. A dimensionless number based on physics and dependent only on input parameters is still needed to make predictions.

In this Letter, we propose a quantitative model for ejection angle prediction from force vector summation: streaming, surface tension, and gravity. Furthermore, we control θ_e beyond 40° across fluid parameters, sessile geometries, and signal parameters [14]. We finally provide a properly balanced, predictive Weber-like dimensionless number.

Experiment.—Typical jetting devices as in Fig. 1 are set up so that signal and sessile drop parameters are well controlled while θ_e is measured. Sessile drops are pipetted onto a hydrophilic region bound by a hydrophobic coating. The hydrophilic region radius, r, dictates the contact angle, θ_c measured from horizontal, for a given volume, V [23]. For the experiments in Fig. 2, a single voltage signal burst is applied to one FIDT at its resonance frequency, f. In the remainder of the experiments, a signal is simultaneously supplied to two opposing FIDTs, each with independently controlled peak-to-peak voltage, V_{pp}, and burst duration, t. We measured the focal spot vibrational velocity, $\dot{\xi}$, for each V_{pp} [16] using laser Doppler vibrometry (Polytec UHF-120). We define the use of two different voltage values in the two signals as the vibrational velocity ratio method

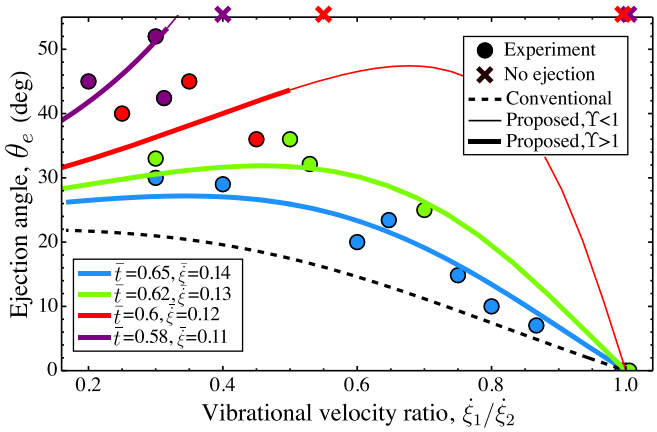

FIG. 3. In order to control θ_e to ≈45° with the vibrational velocity ratio, the average vibrational velocity, $\bar{\dot{\xi}}$, and average duration, $\bar{t}$, must be adjusted. Our proposed model, Eq. (5), explains the experimental results with greater fidelity than the conventional model, Eq. (2), and also indicates which parameter values will produce the desired angles. Notice that greater inertia (increasing $\bar{t}$ or $\bar{\dot{\xi}}$) moves the proposed model closer to the conventional model, confirming as in Fig. 2 that inertia-dominated ejection is limited to θ_R, but θ_e can be much greater with substantial surface tension. Thick lines indicate droplet ejection is predicted via Eq. (6), while thin lines indicate no ejection is predicted.

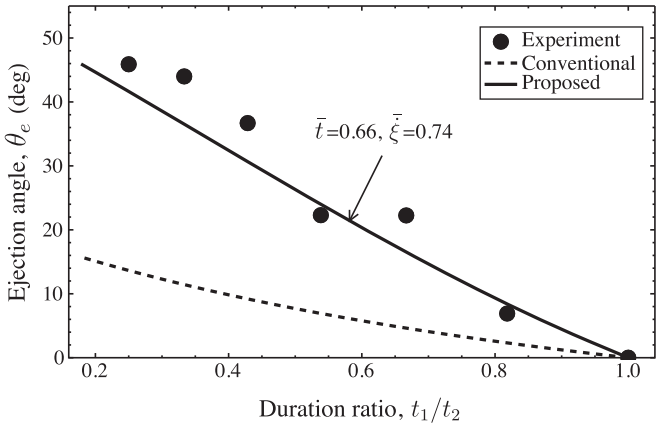

FIG. 4. The duration ratio method achieves ejection control to ≈45° with a fixed parameter set. Our proposed model, Eq. (5), explains the experimental data better than the conventional model, Eq. (2), by accounting for surface tension and gravity. Notably, ejection angle is nearly a linear function of duration ratio, an attractive feature in the context of potential applications, and in distinct contrast to the highly nonlinear relationship present between vibration velocity ratio and ejection angle observed in Fig. 3.

(Fig. 3); the signals are, otherwise, identical. We define the use of two different burst durations in the two signals as the duration ratio method (Fig. 4); in this approach, the signals start simultaneously and are, otherwise, identical, only differing by the time at which they finish. We record each jetting event (Photron Fastcam Mini UX100) at 5000 fps and measure θ_e in postprocessing (ImageJ and MATLAB) [16,17]. Water and aqueous mixtures of glycerol and propylene glycol [16] provide varied viscosities, densities, and surface tensions (see Fig. 5).

Though we investigate their effects, this Letter is not focused on θ_c and f. Doubling f from 40 to 80 MHz produces negligible changes in θ_e [16]. However, varying θ_c from 60° to 100° strongly affects achievable θ_e ranges, with the largest θ_e range when $\theta_c = 75°$ [16]. We also note a strong effect on the ejected droplet number from θ_c—more than from V [18]. Henceforth, we fix $\theta_c = 75°$ and $f = 40$ MHz to enable thorough investigation of other θ_e dependencies.

We investigate a four-dimensional parameter space (Fig. 6) to experimentally determine the null, single, and multiple droplet ejection regimes. Vibrational velocity ratio and duration ratio are important since each controls θ_e. We also choose average vibrational velocity, $\bar{\dot{\xi}} = (\dot{\xi}_1 + \dot{\xi}_2)/2$, and average duration, $\bar{t} = (t_1 + t_2)/2$, since these control total energy input. In each subspace, two parameters were kept constant at values known by the experimenter to produce single droplets while the remaining parameters were varied.

Physical model.—We estimate θ_e via force summation acting on the sessile drop: acoustic streaming, surface tension, and gravity. The acoustic streaming acceleration vector is given by

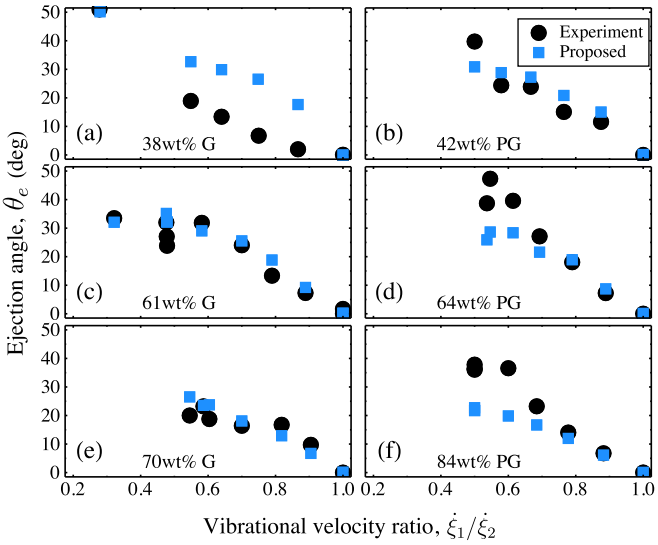

FIG. 5. Aqueous mixtures of glycerol (G) and propylene glycol (PG) were jetted using the vibrational velocity ratio method. As in Fig. 3, $\bar{t}$ and $\bar{\dot{\xi}}$ were adjusted as needed to obtain desired angles. For clarity, we only plot model points necessary for comparison with experiments. Equation (5) takes fluid parameters into account, predicting ejection angle without need for *ad hoc* empirical fitting parameters.

$$\mathbf{A}_s = \frac{\pi v_a^3 f \beta}{2 c_l^2} \mathbf{e}_r, \tag{1}$$

a modified version of the one presented by Tan *et al.* [1], where $v_a = \dot{\xi} e^{-\alpha_l y}$ is the particle velocity due to the passage of the acoustic wave and explicitly dependent upon the vibration velocity $\dot{\xi}$, $\mathbf{e}_r$ is a unit vector along the acoustic wave propagation direction in Fig. 2, and β is the nonlinearity coefficient [24]. Note y is measured along $\mathbf{e}_r$. Acoustic wave absorption by the fluid is described by the length along the substrate over which the leaky Rayleigh wave amplitude attenuates by an exponential factor, $\alpha_r^{-1} = [(\rho_s c_r^2)/(\rho_l c_l f)]$ [25]. The longitudinal sound wave within the fluid has a distinct attenuation length, $\alpha_l^{-1} = \{(\rho_l c_l^3)/[4\pi^2 f^2([4/3]\mu + \mu_b)]\}$ [7], where ρ_l and ρ_s are the density of the liquid and solid, respectively, f is the driving frequency, and μ and μ_b are the dynamic and bulk viscosity, respectively. Each FIDT produces a longitudinal acoustic wave propagating at θ_R from its side of the parent drop [Fig. 1(b)]. Summing these two contributions predicts the angle of the combined acoustic streaming jet

$$\hat{\theta}_e = \arctan\left[\frac{(t_1 A_{s1} - t_2 A_{s2}) \tan\theta_R}{(t_1 A_{s1} + t_2 A_{s2})}\right], \tag{2}$$

representing the conventional model for the droplet ejection angle from past literature [5]. Note that Eqs. (2) and (5) have been rewritten in terms of the vibrational velocity ratio, $\dot{\xi}_1/\dot{\xi}_2$, and the duration ratio, t_1/t_2, for use in

Figs. 3, 4, 5, and 6. Without a fluid interface, Eq. (2) is valid, but for sessile drops, it poorly predicts experimental droplet ejection (Figs. 3 and 4).

We revise the model on the hypothesis that surface tension is responsible for the observed discrepancy. We derive the surface tension term by noting that it acts at the point where streaming jets intersect the drop interface [Fig. 1(b)]. This defines a circle of radius r_s [26], whose circumference gives the force due to surface tension at this point, $\gamma 2\pi r_s$, applied at the local angle of the fluid interface, θ_s [27] measured from the horizontal [Fig. 1(d)]. This force divided by the parent drop mass is the surface tension acceleration

$$\mathbf{D}_{st} = \frac{\gamma 2\pi r_s}{V\rho_l}\mathbf{e}_s, \tag{3}$$

where $\mathbf{e}_s$ is a unit vector pointing along the fluid surface as shown in Fig. 2. The forces do not generally act over the same time period. Streaming acts over burst durations t_1 and t_2, but surface tension and gravity act from initial interface deformation to droplet pinch-off

$$t_{df} = \frac{r - (\alpha_r^{-1}/4)}{\sin(\theta_R)v_a} + \sqrt{\frac{\rho_l r_s^3}{\gamma}}. \tag{4}$$

The second term in Eq. (4) is the characteristic timescale [13], which estimates the time for breakup to occur after column formation. The first term characterizes time taken for column formation, estimated as the distance from the streaming origin to the intersection with the opposite streaming vector divided by v_a. Notice that the jet originates a distance from the three-phase contact line [Fig. 1(b)] due to beam displacement, sometimes called the Schoch length and explained by Bertoni and Tamir [28]. We estimate this quantity based on high speed imaging as $\alpha_r^{-1}/4$. Equation (4) matches high speed observations to an accuracy equivalent to observation accuracy in a representative sample of experiments. And, finally, we note that gravity acts vertically downward with the standard value.

The sum of acceleration vectors produces a prediction of the droplet ejection angle [24]

$$\theta_e = \arctan\left[\frac{(t_1A_{s1} - t_2A_{s2})\sin\theta_R}{(t_1A_{s1} + t_2A_{s2})\cos\theta_R - t_{df}(D_{st}\sin\theta_s/4 + g)}\right]. \tag{5}$$

Note that the horizontal contributions from surface tension cancel out, so that we are left with only the net vertical. The shape of the sessile drop changes over time, necessitating a time-averaged acceleration due to surface tension. The initial, maximum value, D_{st} [Eq. (3)], decays over time with decreasing radius, r_s. High-speed image sequences reveal that r_s decreases cubically, producing the time-averaged value $D_{st}/4$ [16,29].

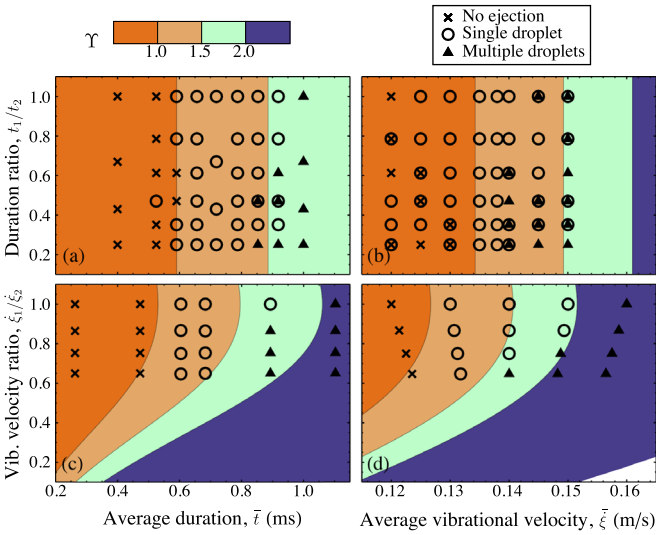

FIG. 6. Adjusting both the vibrational velocity and the burst duration from each FIDT produces a four-dimensional space; (a), (b), (c), and (d) represent four different cross sections of this parameter space. Experiments reveal the single droplet regime in these sectional plots as circles amid either zero or multiple droplet ejections. Equation (6) generates the contours in the background. In all four spaces, the emboldened line indicating $\Upsilon = 1$ coincides with the onset of single droplet events in the experiments.

In addition to θ_e, these accelerations facilitate definition of a dimensionless number for predicting whether zero, one, or multiple droplets will eject. If the ratio [24]

$$\Upsilon = \left[\frac{(t_1A_{s1} + t_2A_{s2})\cos\theta_R}{t_{df}(D_{st}/4 + g)}\right], \tag{6}$$

is greater than one, a droplet is ejected. Once the balance has tipped towards inertia-dominated behavior, experimental data suggest a secondary threshold beyond which multiple droplets are ejected.

Discussion.—Both methods of ejection angle control are effective and both are well described by our model, Eq. (5). Average vibrational velocity and average duration influence the number of droplets as expected (Fig. 6), but they also influence θ_e (Fig. 3). This is because, as in Fig. 2, the strength of streaming relative to surface tension affects θ_e, and streaming depends on both duration [t_i in Eq. (5)] and vibrational velocity [$\dot{\xi}$ in Eq. (1)]. Our proposed model translates this qualitative observation into quantitative understanding.

Ejection angles up to 45° are demonstrated with both methods, but the control parameters must be adjusted in order to achieve this with the vibrational velocity ratio method. This is readily understood in light of our model, as no single curve in Fig. 3 contains the full range, 0°–45°.

Consulting Eqs. (5) and (1), this results directly from nonlinear dependence on v_a with corresponding nonlinear curves in Fig. 3, and linear dependence on t_i with a corresponding linear curve in Fig. 4. These dependencies also influence droplet formation regimes—Figs. 6(a) and 6(b) have vertical contours while Figs. 6(c) and 6(d) have nonlinear contours. The linear nature of the duration ratio method may provide better control in applied settings.

Figure 6 clearly indicates agreement between experiment and the single droplet regime at $\Upsilon = 1$, whereas other definitions require empirical threshold calibration [1]. Similarly, beyond $\Upsilon = 2$ ejection events reliably contain multiple droplets, a threshold which is not built into Eq. (6). Between single and multiple droplet regimes, a transition regime appears at $1.5 < \Upsilon < 2.0$.

Our proposed model accurately predicts θ_e for multiple fluids without relying on any *ad hoc* fitting parameters (Fig. 5) for a majority of the fluids and input signals chosen. There is an apparent offset between experiment and model in Fig. 5(a); there may be an experimental error here since the deviation is consistent in magnitude and direction but absent in most other cases. Jetting higher viscosity fluids requires higher energy input via larger vibrational velocities and/or burst durations. They are more difficult, in practice, to eject at large angles. These features are captured in our proposed model simply by accounting for inherent fluid parameters, leading to reliable mean estimates of observed phenomena. In polymer solutions for 3D printing applications, there is an interesting topic for future research. The viscosity behavior of such non-Newtonian liquids could be determined using SAW-based rheometry [3] and applied to our model. After initial validation, our model could predict polymer droplet jetting angles given only fluid property data on the polymer solutions.

The validity of Eq. (1) for streaming is corroborated by an alternative method starting with the streaming velocity calculated by a form of Lighthill's turbulent jet model modified by Dentry [8]. A simple Newtonian calculation determines the streaming acceleration where the acoustic beams meet, just above the original drop interface. This value, $\approx 60\ \mathrm{m/s^2}$, obtained by independent theoretical means, approximately agrees with the value, $\approx 40\ \mathrm{m/s^2}$, obtained from Eq. (1) with the same parameter set: 40 MHz, 0.74 m/s, 0.65 ms, and water. This agreement is remarkable for such dissimilar approaches given the system's complexity.

The simplicity of our approach, considering its accuracy and the insight it provides into the phenomenon, is an advantage over resource-intensive alternatives. For example, one could consider streaming as a force vector field evolving in time and iterate its effect on interface shape taking into account surface tension at each point via curvature, a much more difficult and time-consuming problem. In other settings, one might also include acoustic radiation pressure, which deforms liquid interfaces [30]. However, the deformations are typically much smaller than those produced here, and moreover, they occur as capillary waves, described by Brunet *et al.* as "trembling" [31], rather than large scale fluid motion. Simulations by Brunet *et al.* show that standing wave patterns have already formed by the time the fluid interface deforms. Such patterns cannot result in millimeter scale deformation at θ_R, which Brunet *et al.* submit is caused by directional, "coherent" acoustics. We argue that this is well described mathematically by acoustic streaming. Further, we point out that particle image velocimetry performed by Dentry *et al.* in the absence of an interface—in which case radiation pressure can have no effect—shows that flow velocities at ~ 1 m/s are generated using SAW streaming at the vibrational velocities used in our experiments [8]. Close agreement between our proposed model and experiment validates our omission of radiation pressure.

The work presented here was generously supported by a SERF research grant to J. Friend from the W. M. Keck Foundation. He is furthermore grateful for the support of this work by the Office of Naval Research (Grant No. 12368098). This work was performed in part at the San Diego Nanotechnology Infrastructure (SDNI) of UCSD, a member of the National Nanotechnology Coordinated Infrastructure, which is supported by the National Science Foundation (Grant No. ECCS–1542148). The authors are grateful to John Roy and team in San Diego from Optec Laser Systems, for substantial training, assistance, and advice throughout this effort.

*Corresponding author.
jfriend@eng.ucsd.edu

[1] M. K. Tan, J. R. Friend, and L. Y. Yeo, Interfacial Jetting Phenomena Induced by Focused Surface Vibrations, Phys. Rev. Lett. **103**, 024501 (2009).

[2] J. C. Brenker, C. Devendran, A. Neild, and T. Alan, On-demand sample injection: combining acoustic actuation with a tear-drop shaped nozzle to generate droplets with precise spatial and temporal control, Lab Chip **20**, 253 2020).

[3] A. G. McDonnell, N. N. Jason, L. Y. Yeo, J. R. Friend, W. Cheng, and R. Prabhakar, Extensional viscosity of copper nanowire suspensions in an aqueous polymer solution, Soft Matter **11**, 8076 (2015).

[4] P. Bhattacharjee, A. McDonnell, R. Prabhakar, L. Yeo, and J. Friend, Extensional flow of low-viscosity fluids in capillary bridges formed by pulsed surface acoustic wave jetting, New J. Phys. **13**, 023005 (2011).

[5] J. O. Castro, S. R. Ramesan, H. D. Dang, A. R. Rezk, and L. Y. Yeo, Acoustopipetting: Tunable Nanoliter Sample Dispensing Using Surface Acoustic Waves, Anal. Chem. **91**, 5621 (2019).

[6] W. Connacher, N. Zhang, A. Huang, J. Mei, S. Zhang, T. Gopesh, and J. Friend, Micro/nano acoustofluidics: materials, phenomena, design, devices, and applications, Lab Chip **18**, 1952 (2018).

[7] J. Lighthill, Acoustic streaming, J. Sound Vib. **61**, 391 (1978).

[8] M. B. Dentry, L. Y. Yeo, and J. R. Friend, Frequency effects on the scale and behavior of acoustic streaming, Phys. Rev. E **89**, 013203 (2014).

[9] S. Shiokawa, Y. Matsui, and T. Ueda, Liquid streaming and droplet formation caused by leaky Rayleigh waves, in *Proceedings, IEEE Ultrasonics Symposium* (IEEE, New York, 1989), pp. 643–646.

[10] P.-G. De Gennes, F. Brochard-Wyart, and D. Quéré, *Capillarity and Wetting Phenomena: Drops, Bubbles, Pearls, Waves* (Springer Science and Business Media, New York, 2013).

[11] J. O. Castro, S. Ramesan, A. R. Rezk, and L. Y. Yeo, Continuous tuneable droplet ejection via pulsed surface acoustic wave jetting, Soft Matter **14**, 5721 (2018).

[12] J. Eggers, Nonlinear dynamics and breakup of free-surface flows, Rev. Mod. Phys. **69**, 865 (1997).

[13] J. Eggers and E. Villermaux, Physics of liquid jets, Rep. Prog. Phys. **71**, 036601 (2008).

[14] See Supplemental Material at http://link.aps.org/supplemental/10.1103/PhysRevLett.125.184504 for a video of droplet ejection at a range of angles, a video comparing effects of contact angle and volume, ImageJ and MATLAB codes used for image processing, the ejection angle and acceleration ratio model code in Mathematica, and a document with further discussion. The document contains the following topics: the affect of sessile drop contact angle on ejection angle, the time averaged radius of the sessile drop where deformation is initiated, the affect of frequency on ejection angle, the vibrational velocity as a function of input voltage, the procedure used to obtain data from high speed imaging, and fluid parameter values (bulk viscosity of water [15], properties of glycerol solutions [16–20], properties of propylene glycol solutions [21,22]).

[15] A. S. Dukhin and P. J. Goetz, Bulk viscosity and compressibility measurement using acoustic spectroscopy, J. Chem. Phys. **130**, 124519 (2009).

[16] L. Bosart and A. Snoddy, Specific gravity of glycerol, Ind. Eng. Chem. **20**, 1377 (1928).

[17] G. P. Association, *Physical Properties of Glycerine and Its Solutions* (Glycerine Producers' Association, New York, 1963).

[18] W. Slie, A. Donfor, Jr., and T. Litovitz, Ultrasonic shear and longitudinal measurements in aqueous glycerol, J. Chem. Phys. **44**, 3712 (1966).

[19] A. Volk and C. J. Kähler, Density model for aqueous glycerol solutions Exp. Fluids **59**, 75 2018.

[20] N.-S. Cheng, Formula for the viscosity of a glycerol-water mixture, Ind. Eng. Chem. Res. **47**, 3285 (2008).

[21] N. G. Tsierkezos and M. M. Palaiologou, Ultrasonic studies of liquid mixtures of either water or dimethylsulfoxide with ethylene glycol, diethylene glycol, triethylene glycol, tetraethylene glycol, 1,2-propylene glycol and 1,4-butylene glycol at 298.15 K, Phys. Chem. Liq. **47**, 447 (2009).

[22] I. S. Khattab, F. Bandarkar, M. Khoubnasabjafari, and A. Jouyban, Density, viscosity, surface tension, and molar volume of propylene glycol + water mixtures from 293 to 323 K and correlations by the Jouyban–Acree model, Arab. J. Chem. **10**, S71 (2017).

[23] V and r are related via the equation for a spherical cap with height, h: $V = \frac{1}{6}\pi h(3r^2 + h^2)$.

[24] M. F. Hamilton, D. T. Blackstock *et al.*, *Nonlinear Acoustics*, Vol. 237 (Academic Press, San Diego, 1998).

[25] R. Arzt, E. Salzmann, and K. Dransfeld, Elastic surface waves in quartz at 316 MHz, Appl. Phys. Lett. **10**, 165 (1967).

[26] r_s is given by the solution of the following system of equations: an offset circle representing the interface, $x^2 + (y + R - h)^2 = R^2$ and a line representing the jet, $y = \cot\theta_R(x + r - \alpha_r^{-1}/4)$. The solution can be put in terms of the sessile drop volume and contact angle via the following equations: $\cos\theta_c = [(R - h)/R]$, $V = [(\pi h^2)/3](3R - h)$.

[27] $\theta_s = \tan^{-1}[(dy)/(dx)]_{x=r_s}$.

[28] H. Bertoni and T. Tamir, Unified theory of Rayleigh-angle phenomena for acoustic beams at liquid-solid interfaces, Appl. Phys. **2**, 157 (1973).

[29] $(1/t_{df})\int_0^{t_{df}} r[(t_{df} - t)/(t_{df})]^3 dt = (r/4)$.

[30] P. L. Marston and R. E. Apfel, Quadrupole resonance of drops driven by modulated acoustic radiation pressure—Experimental properties, J. Acoust. Soc. Am. **67**, 27 (1980).

[31] P. Brunet, M. Baudoin, O. B. Matar, and F. Zoueshtiagh, Droplet displacements and oscillations induced by ultrasonic surface acoustic waves: A quantitative study, Phys. Rev. E **81**, 036315 (2010).